Visnyk NTUU KPI Seriia – Radiotekhnika Radioaparatobuduvannia, 2025, Iss. 100, pp. 27–42

UDC 621.396.969.1

Optimization of Cartesian Feedback Loops for Wideband SDR Transmitters in 5G Mobile Networks

Boiko J. M.[1*], *Pyatin I. S.*[2], *Eromenko O. I.*[1], *Karpova L. V.*[1]

[1]Khmelnytskyi National University, Khmelnytskyi, Ukraine
[2]Khmelnytskyi Polytechnic Professional College by Lviv Polytechnic National University, Khmelnytskyi, Ukraine

E-mail: *boiko_julius@ukr.net*

The article investigates the application of the Cartesian Feedback (CF) loop for distortion compensation in wideband Software-defined radio (SDR) systems, specifically in the context of 5G mobile networks, which incorporate technologies such as Orthogonal Frequency-Division Multiplexing (OFDM) and support applications like the Internet of Things (IoT). The purpose of the research is to minimize nonlinear distortions, such as I/Q-imbalance and phase noise, through a combined analog-digital compensation approach that includes Digital Predistortion (DPD) and the use of a CF loop. In addition, the research aims to investigate how these distortions affect the error resilience of 5G systems, particularly in terms of Error Vector Magnitude (EVM) instability, using Signal-Code Constructions (SCC) based on Quasi-Cyclic Low-Density Parity-Check Code (QC-LDPC) and Polar Codes (P-C) with 256-Quadrature Amplitude Modulation (256-QAM). This dual focus enables a comprehensive analysis of both signal correction mechanisms and their impact on communication reliability. This allows for a significant reduction in computational costs and delays, which is crucial for practical applications in 5G and IoT systems. The object of the study is the effectiveness of the CF loop combined with DPD, analyzed through Simulink Matlab, with an evaluation of its impact on the EVM, Modulation Error Ratio (MER), and Bit Error Ratio (BER). As a result of the research, it is shown that the CF loop enhanced with DPD significantly improves signal quality by reducing EVM and enhancing spectral purity compared to traditional compensation methods such as digital equalization and predistortion.The subject of the research is the optimization of the CF loop for wideband SDR transmitters in 5G mobile networks, aiming to enhance efficiency, reduce latency, and ensure high-quality signal transmission in systems that employ technologies such as OFDM and support IoT applications. The proposed approach enhances the reliability and stability of data transmission in modern wireless networks, which is particularly relevant given the increasing demands for speed and quality of service. The results of this study may be beneficial for telecommunications equipment developers and engineers involved in implementing advanced technologies in the field of wireless communication.

Keywords: 5G; software-defined radio; error vector magnitude; Cartesian feedback; digital predistortion; quasi-cyclic LDPC; modulation error ratio; orthogonal frequency-division multiplexing; internet of things

DOI: 10.20535/RADAP.2025.100.27-42

Introduction. Statement of the problem

In modern Software-defined radio (SDR) systems, particularly in wideband standards such as Orthogonal Frequency-Division Multiplexing (OFDM) [1], 5G New Radio (NR) [2], and Internet of Things (IoT) [3, 4], the problem of nonlinear distortions remains critical. One of the key challenges is the imbalance of quadrature components (I/Q-imbalance), phase noise, and modulation distortion, which significantly degrade the quality of the transmitted signal. For modern high-speed systems, the amplitude imbalance between the I and Q components should not exceed 0.1 dB, while phase imbalance must be within 0.5 degrees. When these values are exceeded, there is a significant increase in the Error Vector Magnitude (EVM), which directly impacts data transmission quality [5].

Traditional distortion compensation methods include digital equalization, adaptive signal processing, and Digital Predistortion (DPD). Equalization corrects distortions using digital filters but requires substantial computational resources and introduces processing delays. Adaptive correction algorithms, such as Least Mean Squares (LMS) or Recursive Least Squares (RLS), dynamically adjust filter parameters to minimize distortions, however, they also require considerable computational power. Predistortion, widely used in power amplifiers (PA), compensates for nonlinearities before signal amplification, but its effectiveness depends on the accuracy of the amplifier model.

One promising approach is the use of Cartesian Feedback (CF) loops, which perform distortion compensation at the analog level, reducing computational costs and delays [6, 7]. This method has already been implemented in several commercial SDR solutions [8].

This paper explores the potential application of CF loops in wideband SDR systems. The primary research objective is to investigate the effectiveness of this approach in minimizing modulation distortions, evaluate its impact on key performance indicators such as EVM[2], Modulation Error Ratio (MER), and Bit Error Ratio (BER), and compare the obtained results with traditional approaches. The study will be conducted in Matlab for various signal scenarios in 5G and IoT, including Quadrature Amplitude Modulation (M-QAM) [9] and Quasi-Cyclic Low-Density Parity-Check Code (QC-LDPC) coding [4, 10], Polar Codes (P-C) [11, 12]. The analysis results will provide conclusions regarding the feasibility of using CF loops in modern wireless communications.

Thus, the problem statement can be formulated as follows: the objective of this study is to analyze the efficiency of applying a CF loop to minimize modulation distortions in broadband SDR systems. The key research tasks include evaluating the impact of the CF loop on critical signal quality metrics such as EVM, MER, and BER, modeling the operation of the CF loop in a MATLAB environment for various 5G and IoT scenarios, particularly for M-QAM modulation and QC-LDPC coding, P-C, comparing the effectiveness of the CF loop with traditional compensation methods such as DPD and adaptive equalization, and determining the feasibility of integrating the CF loop into modern wireless communication systems while considering power consumption and computational complexity constraints.

The results of this study will provide insights into the feasibility of using the CF loop in next-generation 5G mobile networks and OFDM technologies, contributing to the advancement of nonlinear distortion compensation methods in SDR systems.

1 Analysis of research and publications

To address the key issues in this study, we reviewed relevant publications on CF loops in broadband SDR systems. In [6], a CF loop with error correction is proposed to balance linearity and noise, achieving an 8 dB noise improvement in Wideband Code Division Multiple Access (WCDMA) signals. However, its applicability to OFDM, 5G NR, and IoT remains unexplored, as well as its integration with DPD. Similarly, [7] presents an adaptive linearization method for PA, reducing energy consumption significantly, but does not consider CF loops or their combination with DPD for multi-band transmitters. The impact of phase distortions in CF-based amplifier linearization is investigated in [13], where a phase-correction method is proposed. However, its adaptation for broadband signals and integration with digital techniques like DPD are not analyzed. The study in [14] examines CF loops for nonlinear distortion compensation but overlooks quadrature imbalance and phase noise — critical factors in modern SDR systems. In [15], hybrid predistortion techniques are discussed to overcome DPD limitations, emphasizing intermodulation distortion control. Yet, quadrature imbalance, phase noise, and computational costs remain unaddressed. A novel feedback architecture for transmitter linearization is introduced in [16], but its effectiveness beyond WCDMA is not evaluated. Further research [17–20] explores CF loop adaptations for communication systems, highlighting second-order CF linearizers, adaptive modeling of nonlinear PA, and artificial neural network-based feedback modeling.

An analysis of literature from high-ranking journals, conferences, and leading authors shows that many studies focus on improving the linearity and efficiency of PA using CF loops or DPD methods. However, there are noticeable gaps in addressing specific aspects critical for modern 5G, IoT, and OFDM systems. For instance, most works do not consider the impact of phase distortions, quadrature imbalance, or integration with cutting-edge technologies, which are crucial for broadband and SDR systems with high requirements for EVM.

The research presented in this paper offers several important advantages that distinguish it from other works. Firstly, we consider the interaction between CF loops and digital linearization methods, such as DPD, and explore the energy efficiency and impact of phase distortions, which are highly relevant for broadband signals in 5G and IoT. Our study also focuses on minimizing computational costs and delays, which is essential for high-speed communications such as 5G and IoT.

2 Research method

The transmitter with a CF loop is an enhanced version of the traditional feedback transmitter, replacing the amplitude modulator with a quadrature modulator. The use of a quadrature modulator within the automatic control loop not only linearizes the complex transmission coefficient of the transmitter's forward path but also addresses critical issues related to the quality of the modulated signal. This is particularly relevant in modern wireless communications, such as 5G networks [21, 22]. The functional diagram of the transmitter with a CF loop, including the modulator and PA, is shown in Fig. 1.

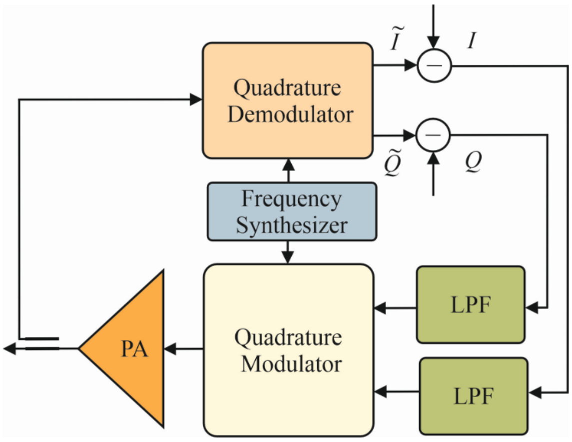

Fig. 1. Functional diagram of linearized transmitter with CF loop: Power Amplifiers (PA), Low Pass Filter (LPF)

The operation of the loop is based on comparing the actual quadrature components of the complex envelope, generated by the processor, with the quadrature components of the complex envelope obtained after demodulating the amplified signal with nonlinear distortions [23].

A portion of the PA output signal is fed to the information input of the quadrature demodulator via a directional coupler. The high-frequency reference signal is supplied to the demodulator from the same frequency synthesizer used to operate the transmitter's quadrature modulator. This ensures the coherence of the quadrature I/Q components received by the error signal detectors from the signal processor and the quadrature I/Q components obtained through demodulation of the amplified modulated signal.

Additionally, a phase shift circuit (not shown in the Fig. 1) compensates for the fixed phase difference between the carrier frequency of the high-PA signal and the carrier frequency of the high-frequency reference signal for the demodulator, including signal propagation delay. In principle, phase correction can be performed not only for the high-frequency modulated signal but also in the low-frequency range for the demodulated quadrature components of the modulated signal.

The error detectors generate independent correction signals based on the reference output quadrature components and the quadrature components obtained from demodulating the distorted amplified high-frequency signal. A low-pass filter suppresses the intrinsic intermodulation frequencies of the error detector and determines the time constant of the CF loop.

In 5G networks, where high data transmission speeds and low latency are crucial, using a quadrature modulator for signal linearization enhances spectral efficiency by reducing interchannel interference (ICI) and achieving a better signal-to-noise ratio (SNR) [24]. Thanks to digital optimization of the baseband signal, modern quadrature modulator chips provide a high level of adjacent channel suppression, meeting electromagnetic compatibility (EMC) standards. This is critical for operation in densely populated spectral environments typical of 5G [25].

Integrating a quadrature modulator into the automatic control loop not only linearizes the modulator and PA but also enables rapid adaptation to changing channel conditions in real time. This ensures stable transmitter parameters, which is essential for maintaining reliable and uninterrupted connections in IoT networks, where signals from a vast number of devices must be transmitted with high reliability.

In the automatic control loop, the input to the comparison element is not the high-frequency modulated signal but the quadrature components of the complex envelope of the modulated signal. This ensures precise and efficient suppression of spurious signals at intermodulation frequencies caused by nonlinearities in the amplifier and modulator, thereby improving transmission quality across different frequency channels.

Notably, this approach enables a high degree of signal linearity, which is a crucial factor in OFDM technologies [26], where any loss of linearity can result in significant distortions due to inter-subcarrier interference (ISI).

The high-frequency voltage at the output of the PA is equal to:

$$U_{out}(t) = \tilde{I}(t)\cos(\omega_c t) + \tilde{Q}(t)\sin(\omega_c t), \tag{1}$$

where $U_{out}(t)$ is the high-frequency modulated signal at the output of the nonlinear PA; $\tilde{I}$, $\tilde{Q}$ are the quadrature components of the complex envelope of the amplified signal.

Equation (1) in its orthogonal form represents the actual high-frequency modulated signal, incorporating nonlinear distortions introduced by the PA and the quadrature modulator.

The high-frequency voltage at the output of the coupler is equal to:

$$U_{out}(t) = K_c\left[\tilde{I}(t)\cos(\omega_c t) + \tilde{Q}(t)\sin(\omega_c t)\right], \tag{2}$$

where K_c is the transmission coefficient of the coupler.

The quadrature demodulator performs the function of converting the spectrum of the real high-frequency signal to the LF range using a complex reference signal (see Fig. 1):

$$V_{ref}(t) = \cos(\omega_c t + \phi_{ref}) + j\sin(\omega_c t + \phi_{ref}), \tag{3}$$

where ϕ_{ref} is the random constant phase of the reference generator.

The ideal matching of the carrier frequency ω_c of the amplified modulated signal (2) with the frequency of the reference generator (3) is achieved by using the same frequency synthesizer for both the modulator and the demodulator, while the nearly zero phase value of the reference generator signal relative to the amplified signal is ensured by the phase compensation circuit.

The phase magnitude remains constant within the frequency band of the modulated signal but changes depending on the operating frequency, according to the overall complex transfer characteristic of the forward path, which includes the quadrature modulator, PA, and coupler. Consequently, a different phase value for the high-frequency reference signal of the demodulator is set according to the current operating frequency.

It is assumed that the quadrature demodulator does not introduce distortion to the demodulated signal. It should be noted that demodulator errors (as with any other component in the feedback loop) are irreparable and must be minimized. The output signal of the quadrature demodulator, taking into account the LPF that suppresses signals at high-order intermodulation frequencies, is the complex envelope of the amplified signal in the low-frequency range:

$$U_{out}(t)=K_cK_{de\ \mathrm{mod}}\left[\tilde{I}(t)\cos\phi_{ref}+\tilde{Q}(t)\sin\phi_{ref}+ \right. \\ \left. +\,j\tilde{Q}(t)\cos\phi_{ref}+j\tilde{I}(t)\sin\phi_{ref}\right], \tag{4}$$

where $K_{de\ \mathrm{mod}}$ is the complex transfer coefficient of the demodulator.

Note that equation (4) assumes that the LPF is transparent in the low-frequency range and does not distort the demodulated signal. Specifically, from (4), it follows that the CF loop must include a phase compensator over the entire possible range of 0–360°. Otherwise, partial conversion of the real part of the quadrature component to the imaginary component, and vice versa, may occur, which would obviously lead to instability in the automatic control loop.

The output signal of the quadrature modulator is a high-frequency modulated signal formed by the error signal between the output signal of the demodulator (4) and the ideal complex envelope $g(t)=I(t)+jQ(t)$ which is generated in the processor. Under conditions of complete phase compensation $\phi_{ref}=0$, then:

$$U_{out}(t)=K_{\mathrm{mod}}\left[I(t)-K_cK_{de\ \mathrm{mod}}\,\tilde{I}(t)\right]\cos(\omega_c t)+ \\ +K_{\mathrm{mod}}\left[Q(t)-K_cK_{de\ \mathrm{mod}}\,\tilde{Q}(t)\right]\sin(\omega_c t), \tag{5}$$

where K_{mod} is the transmission coefficient of the modulator.

Then, we represent the high-frequency modulated signal at the output of the nonlinear PA, which is given by:

$$U_{out}(t)=K_{pa}K_{\mathrm{mod}}\left\{\left[I(t)-K_cK_{de\ \mathrm{mod}}\,\tilde{I}(t)\right]\cos(\omega_c t)+ \right. \\ \left. +\left[Q(t)-K_cK_{de\ \mathrm{mod}}\,\tilde{Q}(t)\right]\sin(\omega_c t)\right\}, \tag{6}$$

where K_{pa} is the transfer coefficient of the nonlinear amplifier.

We performed mathematical transformations and, by combining the expressions for the output signal of the nonlinear PA (1) and (6), we obtain:

$$\begin{aligned}\tilde{I}(t)\left[1+K_{pa}K_{\mathrm{mod}}K_cK_{de\ \mathrm{mod}}\right]&=K_{pa}K_{\mathrm{mod}}I(t),\\ \tilde{Q}(t)\left[1+K_{pa}K_{\mathrm{mod}}K_cK_{de\ \mathrm{mod}}\right]&=K_{pa}K_{\mathrm{mod}}Q(t).\end{aligned} \tag{7}$$

Next, we explicitly presented the previous expressions, where the quadrature components of the complex envelope of the high-frequency modulated signal at the output of the nonlinear PA in the control loop take the following form:

$$\begin{aligned}\tilde{I}(t)&=\frac{K_{pa}K_{\mathrm{mod}}}{1+K_{pa}K_{\mathrm{mod}}K_cK_{de\ \mathrm{mod}}}I(t),\\ \tilde{Q}(t)&=\frac{K_{pa}K_{\mathrm{mod}}}{1+K_{pa}K_{\mathrm{mod}}K_cK_{de\ \mathrm{mod}}}Q(t).\end{aligned} \tag{8}$$

We present expressions (8) as the fundamental equations of the closed-loop automatic control system for the modulator and nonlinear PA with respect to the quadrature components of the modulated signal. The expressions for the error between the quadrature components of the amplified signal and the output (ideal) quadrature components in the closed loop follow from (8) and can be represented in the following mathematical form:

$$\begin{aligned}\delta I&=I(t)-K_cK_{de\ \mathrm{mod}}\,\tilde{I}(t)=\\ &=\frac{I(t)}{1+K_{pa}K_{\mathrm{mod}}K_cK_{de\ \mathrm{mod}}},\\ \delta Q&=Q(t)-K_cK_{de\ \mathrm{mod}}\,\tilde{Q}(t)=\\ &=\frac{Q(t)}{1+K_{pa}K_{\mathrm{mod}}K_cK_{de\ \mathrm{mod}}}.\end{aligned} \tag{9}$$

Thus, with a sufficiently high open-loop gain, expressions (8) transform into the following expressions:

$$\tilde{I}(t)=\frac{I(t)}{K_cK_{de\ \mathrm{mod}}},\qquad \tilde{Q}(t)=\frac{Q(t)}{K_cK_{de\ \mathrm{mod}}}. \tag{10}$$

Well, the expressions (9) for the error signal will have the following format:

$$\delta I(t)\approx 0,\qquad \delta Q(t)\approx 0. \tag{11}$$

The analysis of the obtained equations indicates that expressions (8) and (9) define the transfer characteristics of the quadrature modulator and PA, which are sequentially connected in the automatic control loop for the quadrature components of the modulator's complex envelope in a steady-state mode, under conditions of full phase shift compensation and a transparent LPF for the signal. To analyze the frequency response of the loop and transient processes, it is necessary to specify the expressions for the complex frequency response of the modulator, PA, LPF, and demodulator, along with the total phase angle $\phi_{ref}\neq 0$.

From (10) and (11), in CF loop mode, the modulator and PA achieve near-perfect envelope matching, with the output determined solely by the feedback path — independent of PA and modulator nonlinearities — while imperfections in feedback components limit linearization quality.

We have enhanced the structure of the SDR transmitter with a linearized transmitter by incorporating a CF loop and DPD. The system now has the configuration presented in Fig. 2.

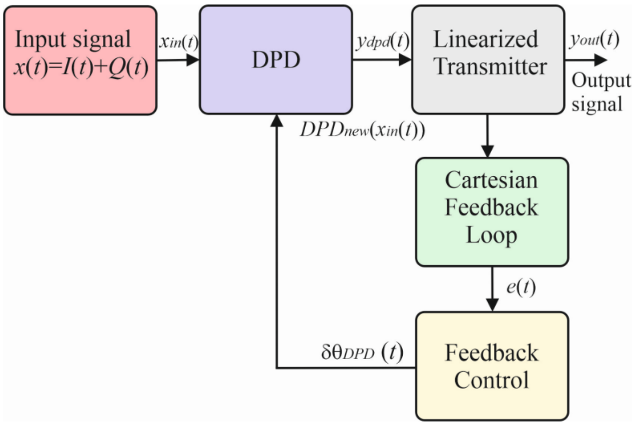

Fig. 2. Adaptive control scheme for SDR transmitter with CF loop and DPD-based linearization

The diagram includes a block that represents the input signal, which is a digital signal to be transmitted. We have modeled it as a complex signal where I and Q are the signal components in the I/Q plane. Following this, there is a block for digital pre-sampling correction DPD. In general, we introduce this block with the aim that it will be responsible for adjusting the transmitted signal in such a way that the compensation of transmitter nonlinearities reduces signal distortion. The next block is the linearized transmitter itself. By linearized transmitter, we mean a transmitter that receives the corrected signal from DPD and transforms it into an analog signal. The schematic format includes a CF loop. Therefore, the characteristic feature is that after the signal is transmitted through the transmitter, the feedback loop receives the signal at the output (for example, via antennas or through channel simulation) and compares it with the original signal to detect and correct distortions. We have also introduced a Feedback Control block. This block compares the output signal with the feedback signal to determine the degree of transmitter nonlinearity, after which it adjusts the DPD parameters to improve the transmitter's linearity. Below, we will show that such a design of the adaptive automatic control system, using DPD and the CF loop (Fig. 2), will enhance the compensation efficiency for both static and dynamic nonlinearities. This is particularly necessary for 5G frequencies and the use of QAM. Furthermore, the presence of high-order terms resulting from large Peak-to-Average Power Ratios (PAPR) in OFDM and QAM creates significant nonlinear distortions due to the limited linearity of the PA. In general, it can be said that 5G NR imposes stringent requirements on EVM and parasitic emission levels (Adjacent Channel Power Ratio, ACPR). Therefore, real-time nonlinear correction using the solutions proposed in the article is essential for solving the scientific problem outlined in the article.

The mathematical description of the system (Fig. 2) in operator form is presented below. Let the input signal be denoted as $x_{in}(t)$, and the corrected output signal of the transmitter as $y_{out}(t)$.

The resampling process for adjusting the operation of the DPD can be mathematically represented by the following equation:

$$y_{DPD}(t) = DPD(x_{in}(t)), \tag{12}$$

where $DPD(x_{in}(t))$ serves as the operator that applies the correction based on DPD algorithms.

The transmission through the linearized amplifier is represented by the following equation:

$$y_{out}(t) = L(x_{DPD}(t)), \tag{13}$$

where $L(x_{DPD}(t))$ is the operator of the linearized transmitter, which converts the corrected signal into an analog signal.

The feedback through the CF loop is represented as follows:

$$e(t) = y_{out}(t) - y_{ref}(t), \tag{14}$$

where $e(t)$ is the error between the transmitter output signal and the feedback $y_{ref}(t)$, which is the desired or expected signal.

The adjustment of the DPD parameters is mathematically described as follows:

$$\delta\theta_{DPD}(t) = \alpha \cdot e(t), \tag{15}$$

where α denotes the correction coefficient, and $\delta\theta_{DPD}(t)$ is a parameter that will reflect the changes made to the DPD algorithm parameters based on the feedback to improve the resampling process.

Accordingly, the update process for the DPD is represented by the following equation:

$$DPD_{new}(x_{in}(t)) = DPD(x_{in}(t), \delta\theta_{DPD}(t)). \tag{16}$$

The process described by equations (16) is adaptively repeated in a loop until the minimum distortion between the output signal and feedback is achieved. Thus, the CF loop with DPD ensures effective linearization of the transmitter, improving signal quality and reducing nonlinear distortions. The results of this improvement will be presented in the experimental section of the article, where we will present studies using signals in real systems.

Automatic control with real-time quadrature synchronization and linear PA adaptation ensures accurate, low-distortion signal transmission in 5G and IoT systems [27].

In the scheme (Fig. 2), we utilized a DPD block for digital predistortion. DPD employs a mathematical model of the amplifier that accounts for both amplitude (AM-AM) and phase (AM-PM) distortions. It analyzes the amplifier's output signal, compares it with the ideal input signal, and applies compensatory corrections to linearize the amplifier. This reduces intermodulation distortions (IMD) and unwanted emissions, lowering the spectral tails and improving system efficiency, as will be shown below.

Overall, DPD has two inputs: one for the direct input signal (see Fig. 2) and another as a reference feedback input from the nonlinear device's output. The DPD architecture can be implemented using the following mechanisms: Memory Polynomial (MP), Dynamic Deviation Reduction of the Second Order (DDR2), Generalized Memory Polynomial (GMP), and Lookup Tables (LUT). The decision-making scheme is based on the least squares method, utilizing the damped Newton algorithm and the step-size reduced damped Newton algorithm for MP, DDR2, and GMP models [28, 29].

Later in this paper, experimental results obtained using the CF model in Simulink will be presented, in which a software-implemented lookup table model with internal generation is applied:

$$y[n] = \sum_{k=0}^{K}\sum_{l=0}^{M} a_{k,l}x[n-l]|x[n-l]|^{k-l}, \tag{17}$$

where K and M are nonlinear order and memory order, respectively. DDR2 models use an input (x) and output (y) relationship given by:

$$\begin{aligned} y[n] = &\sum_{k=0}^{\frac{K-1}{2}}\sum_{l=0}^{M} a_{2k+1,1}[l]|x[n]|^{2k}x[n-l]+ \\ &+\sum_{k=1}^{\frac{K-1}{2}}\sum_{l=1}^{M} a_{2k+1,2}[l]|x[n]|^{2k(k-1)}x^2[n]x^*[n-l]+ \\ &+\sum_{k=1}^{\frac{K-1}{2}}\sum_{l=1}^{M} a_{2k+1,3}[l]|x[n]|^{2k(k-1)}x[n]|x[n-l]|^2+ \\ &+\sum_{k=1}^{\frac{K-1}{2}}\sum_{l=1}^{M} a_{2k+1,4}[l]|x[n]|^{2k(k-1)}x^*[n]x^2[n-l]. \end{aligned} \tag{18}$$

GMP models use an input (x) and output (y) relationship given by:

$$\begin{aligned} y[n] = &\sum_{k=0}^{K-1}\sum_{l=0}^{M-1} a_{k,l}x[n-l]|x[n-l]|^{k}+ \\ &+\sum_{k=1}^{K_b}\sum_{l=0}^{L_b-1}\sum_{l=1}^{M_b} a_{2k,l}x[n-l]|x[n-l-m]|^{k}+ \\ &+\sum_{k=1}^{K_c}\sum_{l=0}^{L_c-1}\sum_{m=1}^{M_c} a_{k,l}x[n-l]|x[n-l+m]|^{k}, \end{aligned} \tag{19}$$

where $K, M, K_b, L_b, M_b, K_c, L_c$, and M_c are model parameters.

Next, we will describe the basic performance indicators that we will use to evaluate the nonlinearity of the PA and the reliability of information reception.

The impact of PA nonlinearity on the reliability of digital signal reception will be determined by the MER parameter and the EVM parameter. Both parameters are used to assess the quality of modulation/demodulation in digital transmitters and receivers and characterize the magnitude of errors introduced by the radio channel to the actual values of the modulated signal [30]. The sources of these errors can include all components of the radio channel, such as the transmitter, the radio wave propagation environment, and the receiver. Specifically, these errors may be caused by parasitic amplitude and phase modulation in the nonlinear PA.

The EVM is the vector difference between the ideal (expected) and actual values of the modulated signal on the state diagram in the orthogonal I/Q coordinate system. The I/Q components define the baseband constellation of the modulated signal, where real and ideal envelopes enable analysis of system distortions by comparing demodulator outputs under ideal and nonideal conditions. The expression for the EVM is given by the difference between the real $v(\tilde{I},\tilde{Q})$ and expected symbol $w(I,Q)$ of the modulated signal:

$$EVM = w(I,Q) - v(\tilde{I},\tilde{Q}). \tag{20}$$

The magnitude of the error vector $EVM = |EVM|$ is defined as the average power of the error vector, normalized to the signal power:

$$EVM = 10\log(P_{err}/P_{ref}), \tag{21}$$

where P_{err} is the root mean square value of the error vector power over the symbol interval T_s; P_{ref} is the maximum power of the expected (ideal) signal in the frequency band.

Graphically, the relationship between the expected (ideal) symbol $w(I,Q)$ vector, the real symbol vector $v(\tilde{I},\tilde{Q})$, and the EVM error vector for binary phase modulation is shown in Fig. 3.

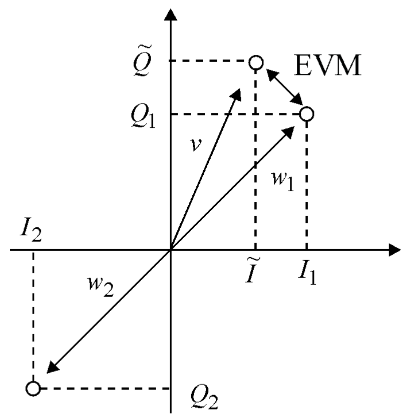

Fig. 3. Diagram illustrating formation of EVM

The real modulated signal is defined by the vector of real states of the modulated signal $\tilde{w}(\tilde{I},\tilde{Q})$, which neither coincides with the vector w_1 nor with the vector w_2.

According to Fig. 3, the magnitude of the error vector is determined by the distance between the orthogonal coordinates of the expected and real values of the modulated signal:

$$EVM = \frac{1}{|w_{\max}|}\sqrt{\frac{1}{N}\sum_{j=1}^{N}\left(I_j - \tilde{I}_j\right)^2 + \left(Q_j - \tilde{Q}_j\right)^2}, \tag{22}$$

where $|w_{\max}| = \sqrt{I_{\max}^2 + Q_{\max}^2}$.

The ratio of the error signal power to the received signal power P_{err}/P_{ref} (18) can be considered as the inverse of the SNR in terms of power, assuming that the magnitude of the error vector takes random values with a root mean square power value $P_{err} = \sigma^2$, where σ^2 is the square of the distribution's variance. Thus, the power ratio P_{err}/P_{ref} can be represented as the ratio of the normalized bit energy of the signal to the spectral power density of the equivalent noise created by the random change in the error vector:

$$\frac{E}{N} = \frac{P_{ref}T_s}{LP_{err}/B} = \frac{BT_s}{L}SNR = \frac{BT_s}{EVM^2 L}, \tag{23}$$

or in logarithmic form:

$$\frac{E}{N} = -20\log\left(EVM\sqrt{\frac{L}{BT_s}}\right), \tag{24}$$

where L is the number of bits per symbol; $SNR = P_{ref}/P_{err}$ is the SNR by power; N is the spectral power density of the equivalent noise.

The obtained expressions (23), (24) will allow us to numerically assess the impact of modulation/demodulation errors on the reliability of information reception. It is worth noting that the classical dependence of reception reliability for FM signals under white noise conditions $BER(E_b/N_0)$ shows that to achieve a reception reliability of 1%, the ratio of normalized bit energy to the spectral power density of white noise must be $E_b/N_0 \geq 8$ dB. It can be assumed that with the error vector magnitude (22) providing a value of $E/N > 20$ dB, the modulation/demodulation errors will have negligible impact on the reliability of digital information reception.

The MER parameter is the ratio of the average power allocated to one symbol to the average power of the symbol detection error and is formally defined by the following expression:

$$MER = \frac{\sum_{j=1}^{N} I_j^2 + Q_j^2}{\sum_{j=1}^{N}\left(I_j - \tilde{I}_j\right)^2 + \left(Q_j - \tilde{Q}_j\right)^2}. \tag{25}$$

We compared the expression (22) for EVM and the expression (25) for MER and established that these parameters are inverse quantities, except for the normalization. The EVM parameter is normalized by the maximum value of the modulus of the expected ideal value of the quadrature component, while the MER parameter is normalized by the root mean square value of all expected ideal values of the quadrature components. The expression for the equivalent SNR introduced by modulation errors (24) is transformed into the following form:

$$\frac{E}{N} = -20\log\left(MER\sqrt{\frac{BT_s}{L}}\right). \tag{26}$$

The algorithm for measuring (calculating) the parameters EVM or MER is straightforward. Using a reference (almost ideal) receiver, the values of the quadrature components are measured (calculated) for all possible information symbols with an almost ideal modulated input signal. Then, the measurements (calculations) are repeated for the modulated signal from the output of the tested PA. If in both cases, the SNR of the modulated signal is much higher than the SNR of the white Gaussian noise, the difference in the measured (calculated) values of the quadrature components is caused only by the influence of the PA. The obtained measurement (calculation) results will be used by us to determine the parameters EVM, MER, or the corresponding equivalent SNR caused by modulation errors.

Modern broadband amplifiers (up to 1 W) allow nearly distortion-free amplification of Quadrature Phase Shift Keying (QPSK) signals up to 100% and $\pi/4$-Differential Quadrature Phase Shift Keying ($\pi/4$-DQPSK) signals up to 70% of $P_{1\text{dB}}$ without compromising reception reliability [31].

To clarify the specifics of the solution we proposed for the control system, let us focus on the following parameters. Specifically, the operation of the PA in the linearization loop (see Fig. 2) will be determined by expression (24), assuming that the amplifier's own noise is neglected:

$$A_{out}(t) = \frac{K_{cntl}K_{pa}(A_{in})}{1 + K_c K_{cntl} K_{pa}(A_{in})} A_{in}(t), \tag{27}$$

where K_{cntl} is the gain coefficient of the control circuit (error detector and amplitude modulator/controlled amplifier); K_c is the transmission coefficient of the output directional coupler; K_{pa} is the gain coefficient of the nonlinear PA.

The error signal detector and the directional coupler are linear devices and are characterized by constant transmission coefficients K_{cntl} and K_c, respectively.

From Fig. 4, we establish that with a relatively low error signal gain of $K_{cntl} = 10$ dB, there can be a significant discrepancy between the envelopes of the input and output signals, leading to weak linearization of the amplifier in the feedback loop. As the error gain increases to 60 dB, the amplifier's operation approaches a linear mode: the first harmonic coefficient rises almost to unity, while the relative level of intermodulation components drops to –70 dB.

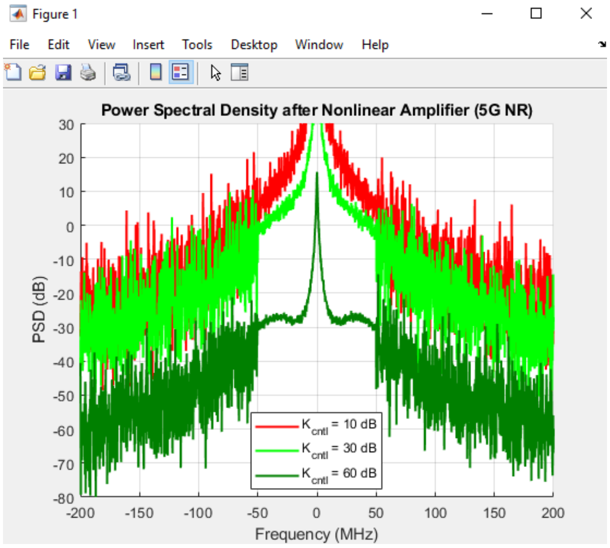

Fig. 4. Output spectrum of linearized amplifier

From the graphs in Fig. 4, we observe that as the error signal gain K_{cntl} increases from 10 dB to 60 dB, spectral fluctuations significantly decrease. For K_{cntl} = 10 dB, the spectral tails exhibit the highest fluctuations, indicating strong nonlinear distortions in the signal. At K_{cntl} = 30 dB, the fluctuations are already significantly reduced, and at K_{cntl} = 60 dB, the spectral tails become even smoother, demonstrating effective amplifier linearization. This behavior highlights the importance of amplifier linearity control for 5G applications, where minimizing nonlinear distortions is crucial for high-quality data transmission at high frequencies.

As an illustration of the variation in out-of-band emissions depending on the feedback coefficient K_c, Fig. 5 shows the output signal spectrum of the linearized amplifier with an error signal gain of 30 dB and a directional coupler transmission coefficient of –10 dB and –50 dB.

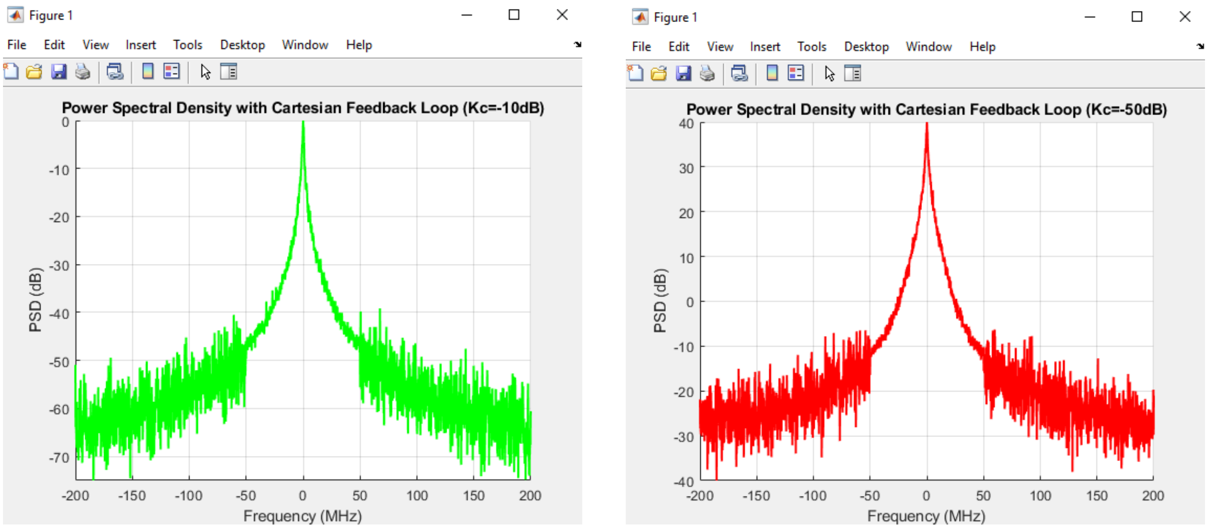

(a) (b)

Fig. 5. Variation of output signal spectrum of linearized amplifier depending on feedback coefficient: (a) Kc = –10 dB; (b) Kc = –50 dB

In the Fig. 6, we present the results of the study on the output signal spectrum of the linearized amplifier for the 5G/IoT frequency scale, taking into account the presence of amplifier phase noise. Figure 6 (a) illustrates the case without a CF loop, emphasizing the actual fluctuation levels of modulation “tails”. Figure 6 (b) presents the study in the case of our proposed automatic control scheme for SDR (Fig. 2) (CF loop+DPD). The spectral representation for our proposed approach (GF+DPD) is shown in blue, while the spectrum without DPD is shown in red.

Below, we provide arguments regarding the obtained results, highlighting the novelty and effects achieved.

According to Fig. 6 (b), the following observations can be made: fluctuations in the modulation “tails” have decreased approximately 2–3 times, reaching ±2 dB instead of ±5–6 dB in the previous case. The level of modulation tails has decreased by approximately 10–15 dB. For example, without DPD, the tails were in the range of –5 to –12 dB, whereas now they approach –40 dB.

The overall reduction in spurious emissions is also observed – the average noise level at side frequencies has improved by 5–8 dB. The result is improved spectral purity, which collectively means reduced distortions and more efficient use of the frequency band. Therefore, the implementation of the CF loop+DPD reduced parasitic effects by 2–3 times and lowered the noise level by 10–15 dB.

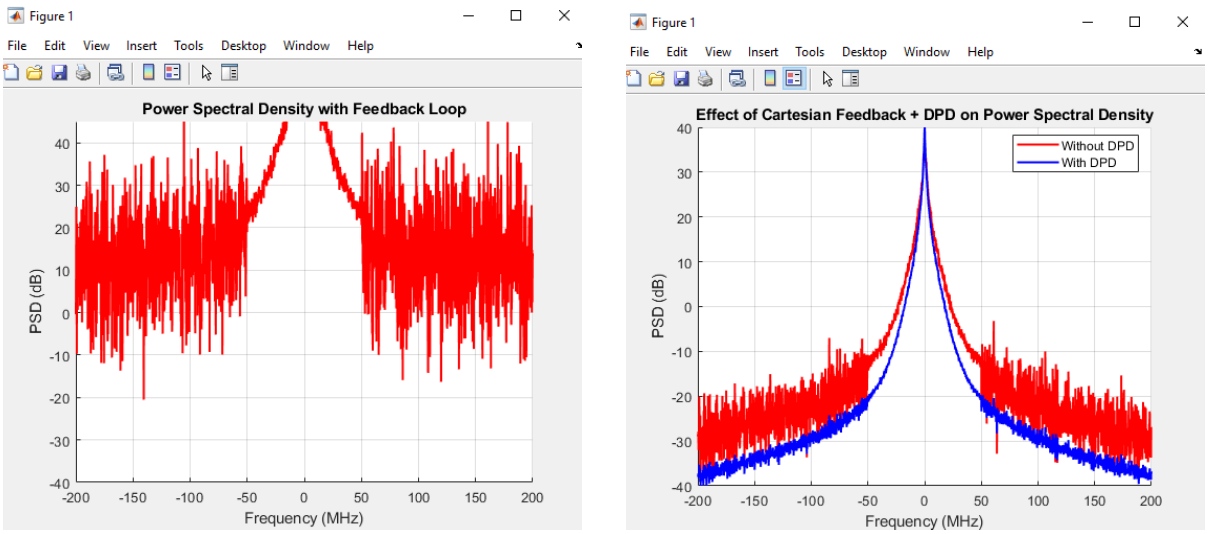

(a) (b)

Fig. 6. Spectrum of the linearized amplifier output signal for the 5G/IoT frequency range, considering amplifier phase noise: (a) without CF loop (showing actual "tail" fluctuations); (b) with the proposed automatic control scheme for SDR transmitter (CF loop + DPD)

Next, we practically illustrate how our proposed solution for optimizing CF works. Specifically, in Fig. 7, we present the spectrum of the output signal of the linearized amplifier for the 5G/IoT frequency scale, taking into account the amplifier's phase noise, with $K_c = -10$ dB.

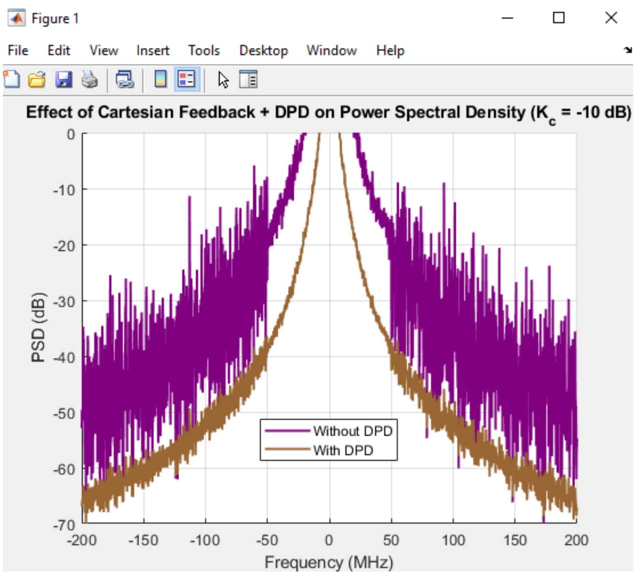

Fig. 7. Spectrum of the linearized amplifier output signal for the 5G/IoT frequency range, considering amplifier phase noise, with $K_c = -10$ dB

Thus, the analysis of Fig. 7 yields the following result. The fluctuations in the divergences have decreased by approximately 2.5–3 times, to ±2 dB from ±5–6 dB in the previous case (red trend, Fig. 6). The modulation tail level has decreased by approximately 10–15 dB — for example, without DPD, the tails reached –55 dB, but now they are in the range of –65...–70 dB. We observe a reduction in the overall level of spurious emissions – the average noise level at the side frequencies has improved by 5–8 dB. We conclude that the spectral purity has improved – overall, this means fewer distortions and more efficient use of the frequency band. In conclusion, the implementation of the CF loop + DPD has reduced the parasitic effects by 2.5–3 times and lowered the noise level by 10–15 dB.

Now, let us consider, with respect to the expression for EVM (19), the errors introduced by nonlinear distortions in the modulated signal. Specifically, from expression (19), it follows that, during one symbol interval, the square of the modulation error vector modulus $|EVM|^2$ is equal to the ratio of the differential signal power to the maximum power.

Accordingly, the magnitude of the modulation error vector $|EVM|^2$ for an amplifier with feedback can be estimated as the square of the difference between the expected signal of the ideal linear amplifier and the real signal (Fig. 4) of the linearized amplifier in the feedback loop, normalized to the maximum power, considering the adopted approximation of the nonlinearity of the gain coefficient $K(A_{in}) = K/(1 + \gamma A_{in})$. Then, the square of the error vector modulus is given by:

$$EVM^2 = \left| \frac{A_{in}K/(1+\gamma A_{in})}{1+HK/(1+\gamma A_{in})} - \frac{KA_{in}}{1+HK} \right|^2 \left| \frac{1+HK}{KA_{in}} \right|^2 = \\ = \left(\frac{KA_{in}}{A_{\max}} \right)^2 \left(\frac{\gamma A_{in}}{1+\gamma A_{in}+HK} \right)^2, \tag{28}$$

where $A_{\max}$ is the maximum output signal; K is the linear gain coefficient; $H = K_c K_{cntl}$ is the open-loop gain coefficient.

Let's consider the methodology for effectively reducing nonlinear distortions in the PA by correcting the quadrature components of the modulating signal. It is assumed that the nonlinear PA is part of a quadrature modulator, to which the quadrature components of the complex envelope and the high-frequency monochromatic signal are applied. The output signal of the nonlinear element (modulator plus amplifier) is represented by an infinite power series according to the main expression:

$$s(t) = \sum_{n=1}^{\infty} a_n \left[\tilde{I}(t)\cos(\omega_c t) + \tilde{Q}(t)\sin(\omega_c t)\right]^n, \quad (29)$$

where $\tilde{I} = I + \delta I$, $\tilde{Q} = Q + \delta Q$ are the quadrature components at the output of the processor; I, Q are the ideal (theoretical) values of the quadrature components; δI, δQ are the differential values between the ideal and real quadrature components; a_n are the approximation coefficients of the total nonlinear characteristic of the modulator and amplifier.

The magnitude of the signals at the third-order combination frequencies in the carrier frequency range of the modulated signal is determined by the expression:

$$\begin{aligned} s_3(t) = a_3 \Big[&3(I+\delta I)^2(Q+\delta Q)\cos^2(\omega_c t)\sin(\omega_c t) + \\ &+ 3(Q+\delta Q)^2(I+\delta I)\sin^2(\omega_c t)\cos(\omega_c t)\Big] \approx \\ &\approx a_3\left[I(IQ + I\delta Q + 2Q\delta I)\sin(\omega_c t) + \right. \\ &\left. + Q(IQ + Q\delta I + 2I\delta Q)\cos(\omega_c t)\right]. \end{aligned} \quad (30)$$

In the case of accurate formation of the quadrature components of the modulating signal $\delta Q = \delta I = 0$, the real values of the quadrature components of the amplified signal αI, αQ are supplemented by signals at third-order combination frequencies, which arise from the nonlinearity of the modulator and the PA and are characterized by the magnitudes of $\approx \alpha_3 Q^2 I$ and $\approx \alpha_3 I^2 Q$, respectively. From expression (30), it follows that when the conditions $\delta I = -I/3$ and $\delta Q = -Q/3$ are simultaneously satisfied, the amplitude of the third-order combination quadrature components is zero. Thus, predistortion of the output quadrature components of the complex envelope according to the modulation law allows suppression of the signals at the combination frequencies.

Next, we define the expression for the EVM through the quadrature components of the complex modulated envelope signal in the CF loop with a nonlinear PA. The magnitude of the EVM is determined by expression (19), taking into account the expression for the error of the quadrature components (9), resulting in:

$$\begin{aligned} EVM^2 &= \frac{1}{|w_{\max}|^2}\sum_{j=1}^{N}\left[I(t)-\tilde{I}(t)\right]^2 + \left[Q(t)-\tilde{Q}(t)\right]^2 = \\ &= \frac{1}{|w_{\max}|^2}\frac{1}{[1+K_{pa}K_{\text{mod}}H]^2}\sum_{j=1}^{N} I_j^2(t) + Q_j^2(t), \end{aligned} \quad (31)$$

where $w_{\max} = (I^2 + Q^2)_{\max}$ is the maximum value of the phase state vector; $H = K_{de\,\text{mod}} K_c$ is the transfer coefficient of the gate.

In the case of nonlinear approximation of the gain coefficient $K_{pa}(A_{in}) = K/(1 + \gamma A_{in})$, equation (31) takes the following form:

$$EVM^2 = \frac{1}{|w_{\max}|^2}\left[\frac{1+\gamma A_{in}}{1+\gamma A_{in} + K_{\text{mod}} KH}\right]^2 \times \\ \times \sum_{j=1}^{N} I_j^2(t) + Q_j^2(t). \quad (32)$$

We can establish that the expression for the error vector (32) in the CF loop qualitatively matches the corresponding expression for the PA in the feedback loop (28). In both cases, the magnitude of the error vector EVM is directly proportional to the relative change in signal power when transmitting different information symbols $\left[I_j^2(t) + Q_j^2(t)\right]/|w_{\max}|^2$, the degree of nonlinearity of the PA, and inversely proportional to the open-loop gain coefficient $K_{\text{mod}} KH$.

A signal of the QAM type (such signals are used in the study area of the article) is characterized by simultaneous changes in both the amplitude and phase of the modulated signal. Accordingly, even in the absence of spectrum limitation, when the I/Q components have constant values over the symbol interval, nonlinear amplification of signals with varying amplitudes over the symbol interval will lead to errors in the modulated signal.

However, it should be noted that in the case of phase modulation with strong spectrum limitation, the magnitudes of the I/Q quadrature components, within the interpretation of trigonometric functions, the amplitude of the input signal $A_{in}^2 = I^2(t) + Q^2(t)$ changes over the symbol interval and varies for different phase states. In this case, there will be a significant impact of the nonlinear amplifier on the parameters of the amplified modulated signal. The acceptable level of distortion will be determined by the equivalent SNR [24], which follows from expression (26), compared to the standard SNR for white Gaussian noise, which defines the allowable error in receiving information.

3 Results

The Fig. 8 shows the constellation diagram for 256-QAM in 5G systems, demonstrating two different scenarios: without the compensation algorithm CF+DPD and with its application, including results obtained using the Simulink model of the proposed compensation circuit. In the first case, when CF+DPD is not applied, a significant spread of points is observed on the diagram, indicating substantial signal distortion. The high EVM^2 (15%) (32) level indicates that the symbols have considerable deviations from their ideal positions, which reduces the accuracy of data transmission. In the second case, when CF+DPD is applied, a significant reduction in distortions is observed. The points corresponding to the received symbols are much closer to the ideal positions. The reduction in EVM^2 (5%) confirms the effectiveness of the algorithm, which compensates for distortions and improves signal quality, leading to more accurate data transmission. This enhances the efficiency of the system, especially under noisy and interference-prone conditions.

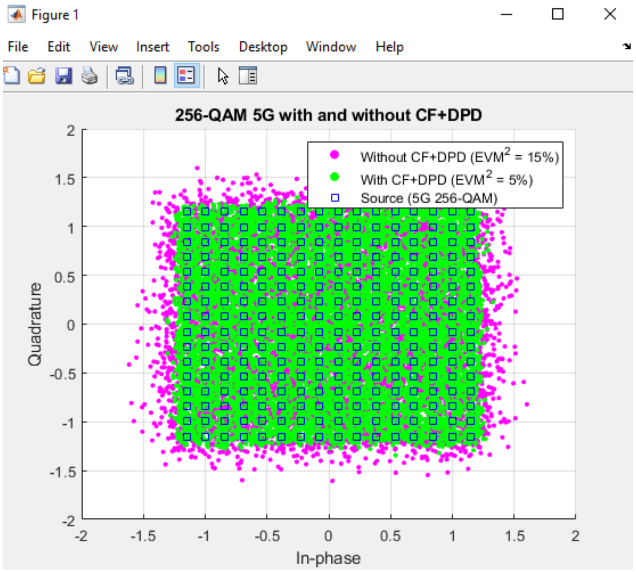

Fig. 8. Constellation diagrams for evaluating EVM^2 under the proposed PA linearization approach based on CF + DPD

The ideal 256-QAM symbol points, marked as blue squares, serve as the reference for comparison with the real values after noise and compensation effects. The high level of accuracy achieved with CF+DPD improves the quality of the connection and increases the system's throughput, which is crucial for the efficient operation of 5G networks.

The constellation diagrams in Fig. 9 illustrate the impact of linearization techniques on the modulation quality of a 256-QAM signal. Specifically, the diagram labeled "256-QAM without CF+DPD" shows that the constellation points are more dispersed, indicating higher levels of distortion and noise within the system. This dispersion reflects a greater deviation of the points from their ideal positions, signifying an increased rate of modulation errors.

In contrast, the "256-QAM with CF+DPD" diagram displays constellation points that are more tightly clustered around their ideal locations. This clustering suggests that the application of CF+DPD effectively compensates for distortions and reduces noise, thereby enhancing signal quality. In a simulated real-world 5G scenario, achieving an EVM^2 (28) of 30% without CF+DPD and 5% with CF+DPD corresponds to MER (25) values of approximately 5.23 dB and 13.01 dB, respectively. These figures demonstrate that the implementation of CF+DPD significantly improves modulation quality by mitigating system distortions and noise [30].

Therefore, both the constellation diagrams and MER values underscore the effectiveness of CF+DPD in enhancing the quality of 256-QAM signals, which is crucial for ensuring reliable data transmission in modern communication systems.

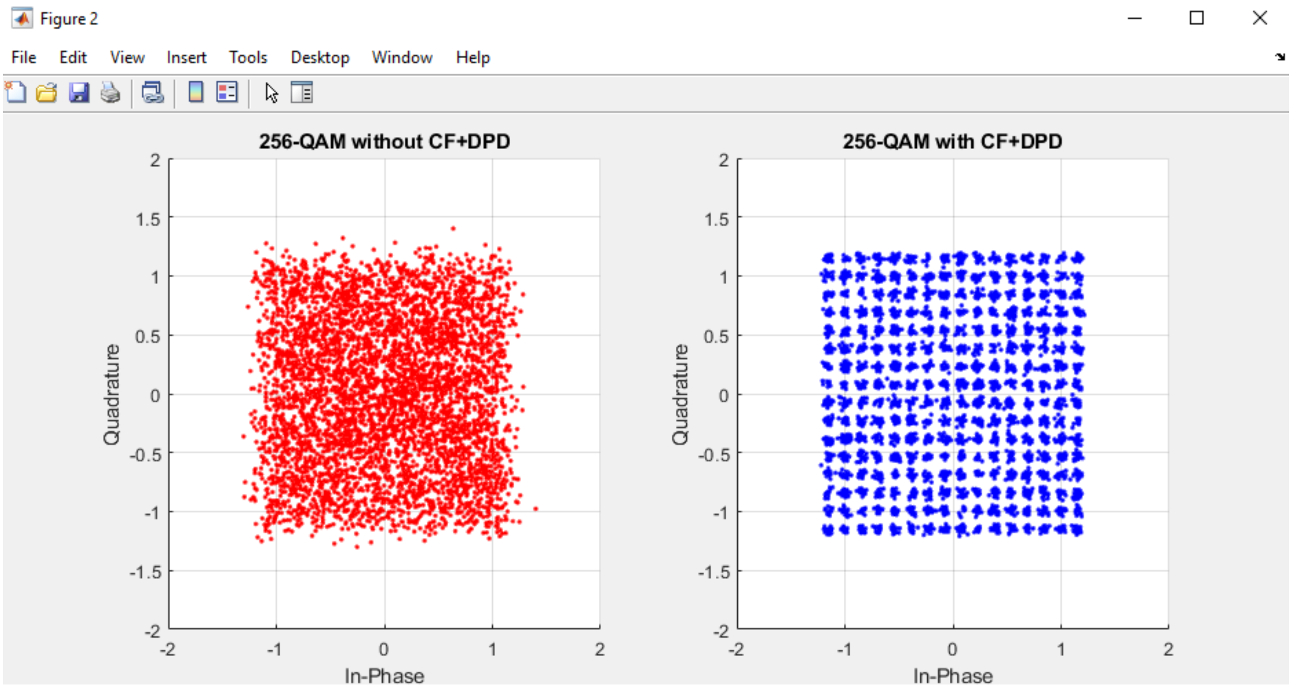

Fig. 9. MER constellation diagrams using the CF + DPD circuit

We utilized expression (24) to numerically assess the impact of modulation/demodulation errors on information reception reliability. Specifically, we investigated the effectiveness of the proposed CF+DPD circuit (Fig. 2). For this study, we selected the following parameters: the number of bits per symbol for 256-QAM (L=8), bandwidth (B=100 MHz), and symbol duration (T_s=1μs), which are standard values for 5G.

Analyzing the EVM versus E/N graph for 256-QAM in 5G systems, the following observations can be made: without CF+DPD at an E/N ratio of 10 dB, the EVM is approximately 30% (or –10.46 dB); with CF+DPD at the same E/N ratio of 10 dB, the EVM decreases to approximately 5% (or –26.02 dB) (Fig. 10 (a)). Thus, the introduction of CF+DPD reduces the EVM from 30% to 5% at a fixed E/N of 10 dB. This corresponds to a sixfold decrease in EVM (or an absolute reduction of 25%). In logarithmic terms, this equates to an improvement of 15.56 dB.

These results clearly indicate that employing CF+DPD in 5G systems with 256-QAM modulation significantly enhances modulation quality, as evidenced by a substantial reduction in EVM at identical E/N values. Ultimately, this enables more reliable data transmission without the need for increased energy expenditure.

In Fig. 10 (b), we also demonstrate how the implementation of the combined CF and DPD circuit we propose in 5G systems with 256-QAM modulation significantly improves signal transmission quality. This is achieved by increasing the MER and correspondingly decreasing the EVM (see Fig. 10 (a)). We observe that without CF+DPD, at E/N=10 dB, the MER is approximately 9.2 dB, whereas with the proposed CF+DPD circuit under the same conditions, the MER increases to 24.5 dB. Overall, this indicates an improvement in MER of 15.3 dB, reflecting a substantial reduction in distortions and an enhancement in system linearity. It is important to note that since MER and EVM are interrelated, an increase in MER leads to a decrease in EVM. The reduction of EVM from 30% to 5% at a fixed E/N=10 dB indicates a significant improvement in modulation accuracy and a reduction in errors in transmitted data. Therefore, the practical conclusion is that the implementation of CF+DPD in 5G systems with 256-QAM modulation significantly enhances signal quality by increasing MER and decreasing EVM. This ensures more reliable and efficient data transmission without the need for increased energy expenditure. We would like to emphasize that the studies presented in Fig. 10 reflect an idealized model and do not account for all possible real-world factors, such as amplifier nonlinearities, phase noise, and interference, which can affect MER in practical scenarios. We present these results to help demonstrate the theoretical foundations and expected system behavior under optimal conditions.

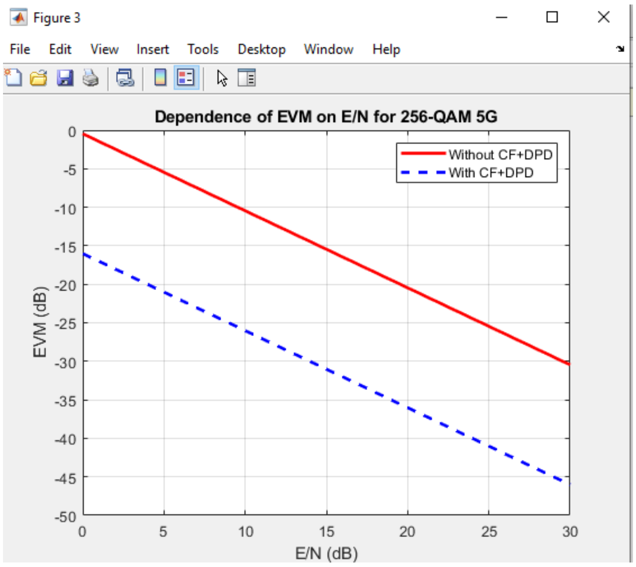

(a)

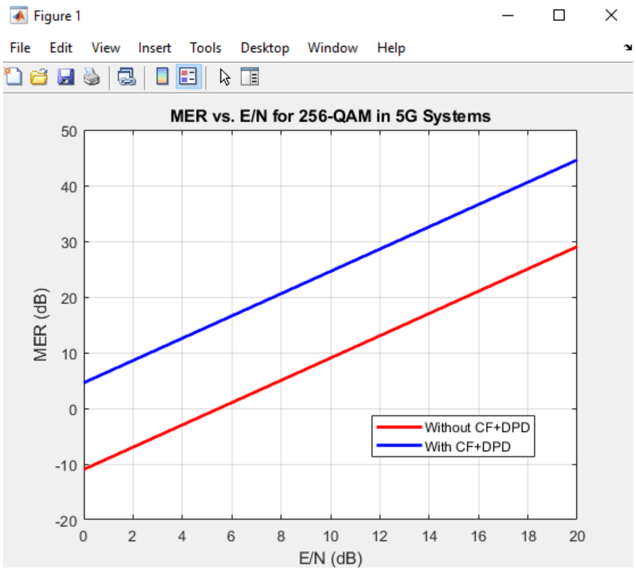

(b)

Fig. 10. Graphs showing impact of modulation/demodulation errors on reception reliability: (a) EVM vs E/N; (b) MER vs E/N using CF+DPD

In Fig. 11 (a, b), we present the results of a study on the noise immunity of the SDR 5G channel using a signal-code construction (SCC) based on QC-LDPC and P-C [32,33]. We investigated how the noise immunity of the channel is affected by optimizing the EVM parameter through the implementation of the CF+DPD structure. In the study of the communication channel with QC-LDPC, we utilized the code rates standard for 5G, namely 0.5 and 0.75. According to 5G NR specifications, we employed codeword lengths of 8448 bits, which corresponds to the maximum allowable length for LDPC in 5G. Additionally, to adjust the required message length, we used shortening and puncturing procedures compliant with 5G NR requirements [2]. Following the recommendations presented in our previous work [4], we applied the Normalized Min-Sum (NMS) decoding algorithm, which is a modified version of Belief Propagation (BP) with message normalization [34, 35]. This approach provided a balance between performance and computational complexity under the conditions of our study. Specifically, we modeled the qualitative impact on the error performance curve (BER vs. E_b/N_0) due to EVM variations resulting from the integration of CF+DPD into the structure of the SDR transmitter. The results are shown in Fig. 11 (a).

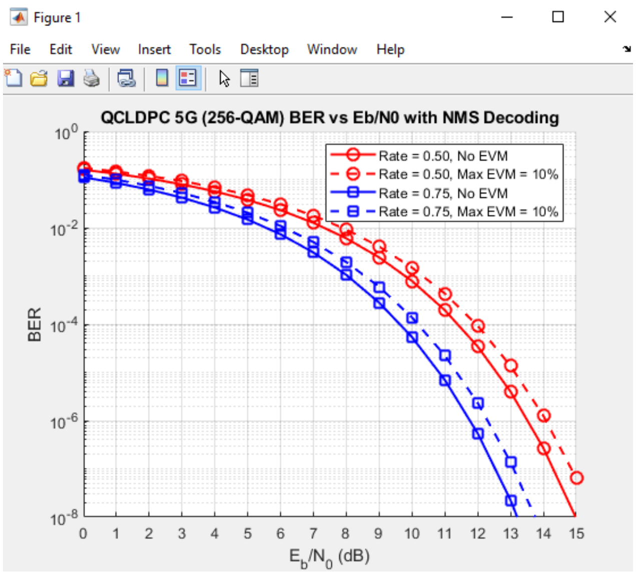

(a)

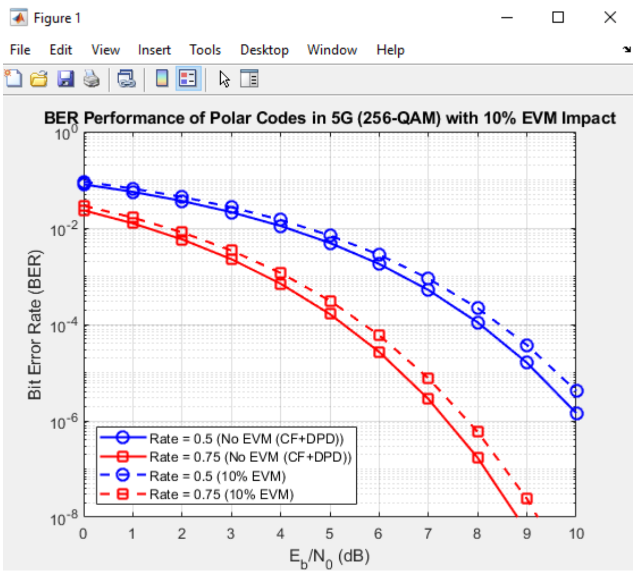

(b)

Fig. 11. BER performance for 5G codes under EVM instability: (a) QC-LDPC+256QAM; (b) P-C+256QAM

The simulation results (Fig. 11 (a)) demonstrate that EVM instability significantly impacts the error performance during transmission using 256-QAM and QC-LDPC 5G. A comparison of the BER curves for the cases without EVM and with maximum EVM=10% shows that even minor EVM instability causes a leftward shift of the curves. This indicates that achieving the same BER level requires a higher E_b/N_0 when EVM is present. Specifically, for the coding rate R=0.5 at BER=10^{-5}, the difference in E_b/N_0 is approximately 0.3 dB, while for R=0.75, it is about 0.4 dB. This shows that EVM increases the system's noise immunity requirements, thus reducing its energy efficiency. How this practically affects the quality of service is discussed in detail in the "Conclusions" section.

For the analysis of P-C (Fig. 11 (b)), we used a code length of N=2048, which is a baseline for 5G. The code rates were set to R=0.5 and R=0.75, respectively. Additionally, the lifting factor (LF) for the P-C was chosen as L=4 (22) and the BP decoding algorithm was employed. The analysis showed that using the CF with DPD reduced the impact of EVM instability on the error resilience of P-C in 5G (256-QAM), achieving a gain of 0.41 dB for the rate of 0.5 and 0.4 dB for the rate of 0.75 at a BER level of 10^{-5}. This demonstrates the effectiveness of the proposed approach, as the EVM improvement mitigated phase and amplitude distortions, leading to better constellation resolution in QAM (shown in Fig. 8 and 9) and, consequently, enhanced energy efficiency of the system without altering the coding rate or transmitter power.

Conclusions

The paper presents a comprehensive study of a combined analog-digital compensation method involving a CF loop and DPD to mitigate nonlinear impairments such as I/Q-imbalance and phase noise. It further investigates the impact of residual EVM instability on the error resilience of 5G systems employing SCC schemes based on QC-LDPC and P-C with 256-QAM modulation. A power amplifier linearization scheme based on the combination of CF and DPD is proposed and evaluated. Simulation results demonstrated that the application of CF+DPD significantly reduces the EVM level (from 30% to 5% at a fixed E/N=10 dB), which corresponds to an improvement in signal modulation quality and an increase in MER by 15.3 dB. This enables more accurate data transmission without increasing energy costs. The study of the impact of EVM instability on error resilience showed that even minor EVM instability causes the BER curves to shift to the right, requiring an increase in E_b/N_0 to achieve the same bit error rate. Specifically, for QC-LDPC with code rates of 0.5 and 0.75, the energy budget losses reach 0.3 dB and 0.4 dB, respectively. This confirms that the use of CF+DPD improves error resilience by minimizing phase and amplitude distortions, which is particularly important for 5G systems using the high-density 256-QAM constellation.

Further research will focus on optimizing DPD by exploring alternative architectures and algorithms for updating LUTs to further reduce EVM. An important direction is the use of machine learning methods for adaptive adjustment of CF+DPD parameters in real-time, depending on channel conditions. This will enhance system efficiency and flexibility in dynamic transmission environments. Additionally, the implementation of CF+DPD in Field-Programmable Gate Array (FPGA) [11, 22] or Application-Specific Integrated Circuit (ASIC) is planned for use in real SDR transmitters to reduce latency and improve energy efficiency. This is critical for deploying high-speed 5G transmitters with low latency, which is essential for URLLC (Ultra-Reliable Low Latency Communications) applications. Considering the rapid development of 5G technologies, it is also reasonable to investigate the efficiency of CF+DPD for other modulation types, such as 1024-QAM, which are increasingly used in modern 5G NR systems. In this context, modeling of the impact of power amplifier nonlinearities, phase noise, and inter-channel interference on the efficiency of the proposed method will be conducted.

The obtained results have significant practical implications for improving efficiency and service quality in 5G networks, including reducing buffering frequency and enhancing real-time video quality. Implementing CF+DPD with new approaches will provide enhanced error resilience and energy efficiency, which are key requirements for future generations of wireless networks.

References

[1] Marey, M. & Mostafa, H. (2021). Turbo Modulation Identification Algorithm for OFDM Software-Defined Radios. *IEEE Communications Letters*, Vol. 25, No. 5, pp. 1707–1711. doi:10.1109/LCOMM.2021.3054590.

[2] Ghosh, A., Maeder, A., Baker, M., & Chandramouli, D. (2019). 5G Evolution: A View on 5G Cellular Technology Beyond 3GPP Release 15. *IEEE Access*, Vol. 7, pp. 127639–127651. doi:10.1109/ACCESS.2019.2939938.

[3] Singh, B. K., Khatri, N. (2024). Enhancing IoT connectivity through spectrum sharing in 5G networks. *International Journal of System Assurance Engineering and Management*, Vol. 15, No. 10, pp. 5018–5029. doi:10.1007/s13198-024-02515-4.

[4] Boiko, J., Pyatin, I., Eromenko, O., & Karpova, L. (2024). Evaluation of the Capabilities of LDPC Codes for Network Applications in the 802.11ax Standard. *IoT Based Control Networks and Intelligent Systems. Lecture Notes in Networks and Systems*, Springer: Singapore, Vol. 789, pp. 369–383. doi:10.1007/978-981-99-6586-1_25.

[5] Abdulwahhab Mohammed, A. & Abdulwahhab, A.H. (2024). Analysis of potential 5G transmission methods concerning Bit Error Rate. *AEU - International Journal of Electronics and Communications*, Vol. 184, pp. 155407. doi:10.1016/j.aeue.2024.155407.

[6] Li, J., Xu, Z., Hong, W., & Gu, Q. J. (2018). A Cartesian Error Feedback Architecture. *IEEE Transactions on Circuits and Systems I: Regular Papers*, Vol. 65, No. 3, pp. 1133–1142. doi:10.1109/TCSI.2017.2761394.

[7] Chung S., Holloway, J. W., & Dawson, J. L. (2008). Energy-Efficient Digital Predistortion With Lookup Table Training Using Analog Cartesian Feedback. *IEEE Transactions on Microwave Theory and Techniques*, Vol. 56, No. 10, pp. 2248–2258. doi:10.1109/TMTT.2008.2003139.

[8] Falcon III RF-7800V-HH Handheld VHF Tactical Radio. Product details. *L3Harris Technologies*, last accessed Apr. 16, 2025.

[9] Al-Rubaye, G. A. (2023). Performance of 5G NR-polar QAM-OFDM in nonlinear distortion plus Non-Gaussian noise over Rayleigh fading channel. *AEU - International Journal of Electronics and Communications*, Vol. 171, pp. 154929. doi:10.1016/j.aeue.2023.154929.

[10] Anandkumar, D., & Sangeetha, R. G. (2022). Performance Evaluation of LDPC-Coded Power Series Based Malaga (M) Distributed MIMO/FSO LinkWith M-QAM and Pointing Error. *IEEE Access*, Vol. 10, pp. 62037–62055. doi:10.1109/access.2022.3180835.

[11] Pyatin, I., Boiko, J., & Eromenko, O. (2024). Algorithmization and Hardware Implementation of Polar Coding for 5G Telecommunications. *Transport and Telecommunication Journal*, Vol. 25, Iss. 3, pp. 300–310. doi:10.2478/ttj-2024-0022.

[12] Sun, H., Viterbo, E., Dai, B., & Liu, R. (2024). Fast Decoding of Polar Codes for Digital Broadcasting Services in 5G. *IEEE Transactions on Broadcasting*, Vol. 70, Iss. 2, pp. 731–738. doi:10.1109/tbc.2023.3345642.

[13] Faulkner, M. (2000). An automatic phase adjustment scheme for RF and Cartesian feedback linearizers. *IEEE Transactions on Vehicular Technology*, Vol. 49, Iss. 3, pp. 956–964. doi:10.1109/25.845112.

[14] Kerhervé, E., & Belot, D. (2015). Linearization and Efficiency Enhancement Techniques for Silicon Power Amplifiers. *Academic Press (Elsevier)*, 154 p. doi:10.1016/c2013-0-00513-0.

[15] Rawat, K., Roblin, P., & Koul, S. K. (2020). Digital Techniques for Broadband and Linearized Transmitters. *Analog Circuits and Signal Processing, Springer International Publishing*, pp. 301–350. doi:10.1007/978-3-030-38866-9_5.

[16] Li, J., & Gu, Q. J. (2017). A low-noise cartesian error feedback architecture. *2017 IEEE International Symposium on Circuits and Systems (ISCAS)*, pp. 1-4. doi:10.1109/iscas.2017.8050253.

[17] Ock, S., Song, H., & Gharpurey, R. (2015). A Cartesian feedback-feedforward transmitter IC in 130nm CMOS. *2015 IEEE Custom Integrated Circuits Conference (CICC)*, pp. 1-4. doi:10.1109/cicc.2015.7338483.

[18] Cavers, J. K., Mehrotra, K., & Woodward, G. K. (2019). Advantages of Second-Order Cartesian Feedback Linearizers for Radio Amplifiers. *IEEE Transactions on Circuits and Systems I: Regular Papers*, Vol. 66, Iss. 11, pp. 4134–4146. doi:10.1109/tcsi.2019.2926387.

[19] Vaskovic, M., Kodogiannis, V. S., & Budimir, D. (2018). An adaptive fuzzy logic system for the compensation of nonlinear distortion in wireless power amplifiers. *Neural Computing and Applications*, Vol. 30, pp. 2539–2554. doi:10.1007/s00521-017-2849-3.

[20] Cárdenas-Valdez, J. R., Núñez-Pérez, J. C., Galaviz-Aguilar, J. A., Calvillo-Téllez, A., Gontrand, C., et al. (2015). Modeling memory effects in RF power amplifiers applied to a digital pre-distortion algorithm and emulated on a DSP-FPGA board. *Integration*, Vol. 49, pp. 49–64. doi:10.1016/j.vlsi.2014.12.005.

[21] Chettri, L., & Bera, R. (2020). A Comprehensive Survey on Internet of Things (IoT) Toward 5G Wireless Systems. *IEEE Internet of Things Journal*, Vol. 7, No. 1, pp. 16-32. doi:10.1109/jiot.2019.2948888.

[22] Boiko, J., Druzhynin, V., Buchyk, S., Pyatin, I., & Kulko, A. (2024). Methodology of FPGA Implementation and Performance Evaluation of Polar Coding for 5G Communications. *CEUR Workshop Proceedings*, Vol. 3654, pp. 15-24.

[23] Wang, X., Wang, J., Shen, Y., Shen, B., & Zhao, M. (2024). Low-Dimensional Post-Distortion for Nonlinear Power Amplifier in MIMO Systems. *Wireless Personal Communications*, Vol. 139, Iss. 3, pp. 1593–1605. doi:10.1007/s11277-024-11675-2.

[24] Pyatin, I., Boiko, J., Eromenko, O., & Parkhomey, I. (2023). Implementation and analysis of 5G network identification operations at low signal-to-noise ratio. *TELKOMNIKA (Telecommunication Computing Electronics and Control)*, Vol. 21, Iss. 3, pp. 496-505. doi:10.12928/telkomnika.v21i3.22893.

[25] Babalola, A. H., Abdulkarim, O. A., Salihu, S. A., & Adebakin, T. O. (2024). Performance Analysis of MIMO-OFDM Systems in 5G Wireless Networks. In: Florez, H., Astudillo, H. (eds) Applied Informatics. ICAI 2024. *Communications in Computer and Information Science*, Vol 2237, pp. 278–291. doi:10.1007/978-3-031-75147-9_19.

[26] Boiko, J., Eromenko, O., Kovtun, I., & Petrashchuk, S. (2019). Quality Assessment of Synchronization Devices in Telecommunication. *2019 IEEE 39th International Conference on Electronics and Nanotechnology (ELNANO)*, pp. 694-699. doi:10.1109/ELNANO.2019.8783438.

[27] Oladimeji, T. T., Kumar, P., & Oyie, N. O. (2022). Propagation path loss prediction modelling in enclosed environments for 5G networks: A review. *Heliyon*, Vol. 8, Iss. 11, ph. e11581. doi:10.1016/j.heliyon.2022.e11581.

[28] Kim, J., & Konstantinou, K. (2001). Digital predistortion of wideband signals based on power amplifier model with memory. *Electronics Letters*, Vol. 37, No. 23, pp. 1417-1418. doi:10.1049/el:20010940.

[29] Morgan, D. R., Ma, Z., Kim, J., Zierdt M. G., & Pastalan, J.(2006). A Generalized Memory Polynomial Model for Digital Predistortion of RF Power Amplifiers. *IEEE Transactions on Signal Processing*, Vol. 54, No. 10, pp. 3852-3860. doi:10.1109/TSP.2006.879264.

[30] Boiko, J., Kovtun, I., & Petrashchuk, S. (2017). Productivity of telecommunication systems with modified signal-code constructions. *2017 4th International Scientific-Practical Conference Problems of Infocommunications. Science and Technology (PIC S&T)*, pp. 173-178. doi:10.1109/INFOCOMMST.2017.8246374.

[31] Mohamed, K. S. (2021). Hardware Realization of DPSK-Based Bluetooth Modem. *Bluetooth 5.0 Modem Design for IoT Devices*, Springer International Publishing, pp. 75–92. doi:10.1007/978-3-030-88626-4_4.

[32] Zhang, Y., & Jiang, M. (2023). Genetic optimization of 5G-NR LDPC codes for lowering the error floor of BICM systems. *Physical Communication*, Vol. 58, pp. 102009. doi:10.1016/j.phycom.2023.102009.

[33] Boiko, J., Pyatin, I., & Eromenko, O. (2024). Development of SC Polar Decoder Design Scenario for 5G/6G Telecommunications Applications. *2024 IEEE 17th International Conference on Advanced Trends in Radioelectronics, Telecommunications and Computer Engineering (TCSET)*, pp. 1-6. doi:10.1109/TCSET64720.2024.10755649.

[34] Jan, Q., Hussain, S., Pan, Z., Liu, N., Ali, Z., Liu, Z., & You, X. (2023). Parity-check and G-matrix based intelligent early stopping criterion for belief propagation decoder for polar codes. *Digital Communications and Networks*, Vol. 9, Iss. 5, pp. 1148-1156. doi:10.1016/j.dcan.2022.12.011.

[35] Boiko, J., Pyatin, I., & Eromenko, O. (2022). Analysis of Signal Synchronization Conditions in 5G Mobile Information Technologies. *2022 IEEE 16th International Conference on Advanced Trends in Radioelectronics, Telecommunications and Computer Engineering (TCSET)*, pp. 01-06. doi:10.1109/TCSET55632.2022.9766899.

Оптимізація картезіанської петлі зворотного зв'язку для систем широкосмугових SDR-передавачів у мережах мобільного зв'язку 5G

Бойко Ю. М., Пятін І. С., Єрьоменко О. І., Карпова Л. В.

У статті досліджується застосування картезіанської петлі зворотного зв'язку (Cartesian Feedback, CF) для компенсації спотворень у широкосмугових системах радіозв'язку з програмно-конфігурованою архітектурою (Software-defined radio, SDR), зокрема в контексті мобільних мереж п'ятого покоління (5G), які включають технології ортогонального частотного мультиплексування (Orthogonal Frequency-Division Multiplexing, OFDM) та підтримують застосування Інтернету речей (Internet of Things, IoT). Метою дослідження є мінімізація нелінійних спотворень, таких як дисбаланс I/Q-складових і фазовий шум, за допомогою комбінованого аналого-цифрового підходу до компенсації, який передбачає використання цифрового передспотворення (Digital Predistortion, DPD) у поєднанні з петлею CF. Крім того, у межах дослідження проаналізовано вплив цих спотворень на завадостійкість систем 5G, зокрема на нестабільність величини вектора помилки (Error Vector Magnitude, EVM), із застосуванням сигнально-кодових конструкцій (Signal-Code Constructions, SCC), побудованих на основі квазіциклічних кодів з низькою щільністю перевірок парності (Quasi-Cyclic Low-Density Parity-Check Code, QC-LDPC) та полярних кодів при застосуванні модуляції 256-QAM (Quadrature Amplitude Modulation). Такий подвійний акцент дає змогу всебічно оцінити як механізми корекції сигналу, так і їхній вплив на надійність передавання інформації. Запропонований підхід дозволяє суттєво зменшити обчислювальні витрати та затримки, що є критично важливим для практичного використання у системах 5G та додатках IoT. Об'єктом дослідження є ефективність петлі CF у поєднанні з DPD, проаналізована в середовищі Simulink Matlab із врахуванням впливу на величину вектора помилки (EVM), коефіцієнт похибки модуляції (Modulation Error Ratio, MER) та ймовірність бітової помилки (Bit Error Ratio, BER). У результаті дослідження показано, що петля CF у комбінації з DPD суттєво покращує якість сигналу, зменшуючи EVM та підвищуючи спектральну чистоту порівняно з традиційними методами компенсації, такими як цифрова еквалізація та передспотворення. Предметом дослідження є оптимізація петлі картезіанської петлі зворотного зв'язку для широкосмугових SDR-передавачів у мобільних мережах 5G з метою підвищення ефективності, зменшення затримок та забезпечення високої якості передавання сигналу в системах, що використовують технології OFDM і підтримують IoT-додатки. Запропонований підхід підвищує надійність і стабільність передавання даних у сучасних бездротових мережах, що особливо актуально з огляду на зростаючі вимоги до швидкості та якості обслуговування. Результати дослідження можуть бути корисними для розробників телекомунікаційного обладнання та інженерів, які займаються впровадженням передових технологій у сфері бездротового зв'язку.

Ключові слова: 5G; програмно-конфігуроване радіо (SDR); величина вектору помилки (EVM); картезіанський зворотний зв'язок (CF); цифрова передкорекція (DPD); квазіциклічні коди низької щільності перевірок на парність (QC-LDPC); коефіцієнт помилки модуляції (MER); ортогональне частотне мультиплексування (OFDM); інтернет речей (IoT)